ABSORPTION AND FLUORESCENCE SPECTROSCOPIC ANALYSIS
USING COMPACT, LINEAR VARIABLE FILTER BASED,
DETECTION PLATFORMS

BY

SAOUD A. AL-MULLA

THESIS

Submitted in partial fulfillment of the requirements
for the degree of Master of Science in Electrical and Computer Engineering
in the Graduate College of the
University of Illinois at Urbana-Champaign, 2017

Urbana, Illinois

Advisers:

    Associate Professor John M. Dallesasse
    Professor Brian T. Cunningham

ABSTRACT

Spectroscopic analysis is an integral part of biological and chemical sensing. However, most spectroscopic equipment is relegated to laboratories. Compact and portable alternatives to conventional spectroscopic tools allow for testing outside of laboratory settings. This is achieved by making the underlying equipment affordable and easy to use while preserving reasonable accuracy and sensitivity. Due to their ubiquity, and constantly improving hardware and software, smartphones represent a favorable candidate for integration with spectroscopic technologies. This work presents the design, fabrication and characterization of compact measurement platforms capable of both absorption and fluorescence spectroscopic analysis using linear variable filters (LVF). The platform's potential for integration into next generation smartphones is demonstrated by the use of a conventional CMOS image sensor in conjunction with the LVF to create the detection element. An LVF-based benchtop detection setup is initially presented followed by its miniaturized successors: compact absorption and fluorescence detection platforms. A series of tests is discussed, most notably an enzyme-linked immunosorbent assay used to measure concentrations of human fetal fibronectin, a predictor of preterm birth, as a real-world contextualization of the absorption platform.

ACKNOWLEDGMENTS

I would like to thank a few people who made this work possible.

My parents and my aunt Natasha, for their unwavering support from across the pond (and then some).

My friends, for making my six years in Champaign unforgettable, leaving me with many fond memories, and who I am very much looking forward to seeing again now that my thesis is submitted.

Char, for her moral support throughout the process of writing this work, and for letting me pace around her apartment until I could pace no longer and had to start writing instead.

The Dallesasse and Cunningham groups for their camaraderie and guidance over the last two years.

Tommy, John and Patrick, for their discussions, candor and friendship, as well as some much needed coffee breaks.

The group mates, past and present who worked on the Lab-in-a-Smartphone project, particularly Yuhang Wan. Yuhang's leadership and nous, coupled with the group's perseverance, work ethic and collaborative spirit allowed us to successfully turn a concept into a series of working devices.

My professors, John Dallesasse and Brian Cunningham for their guidance, encouragement and mentorship. The lessons I learned from them and their groups will undoubtedly benefit me for the rest of my life.

The National Science Foundation for funding the work presented in this thesis.

Kuwait, for financially supporting me throughout my higher education.

TABLE OF CONTENTS

LIST OF ABBREVIATIONS

CMOS   Complementary Metal-Oxide Semiconductor

ELISA   Enzyme Linked Immunosorbent Assay

LED   Light-Emitting Diode

LVF   Linear Variable Filter

NIR   Near-Infrared

OSA   Optical Spectrum Analyzer

POC   Point-of-care

QD   Quantum Dot

SNR   Signal-to-noise Ratio

VIS   Visible

CHAPTER 1

INTRODUCTION

1.1   Motivation

Spectroscopic analysis plays an important role in biological and chemical sensing. It has successfully been utilized in a wide variety of fields ranging from environmental sensing [1], [2], [3], [4], [5] to medical diagnostics [6], [7], [8], [9], [10], [11]. However, spectroscopy equipment is generally relegated to laboratories as its bulk and high cost are not conducive to field analysis. Interest in point-of-care (POC) diagnostics, motivated in part by the desire to bring lab-quality testing to regions without access to dedicated laboratories, has called for the advent of portable alternatives [12]. Compact and portable alternatives to conventional laboratory tools promise to increase access to diagnostic tests by making the underlying equipment affordable and easy to use with comparable accuracy and sensitivity.

A suite of commercial portable spectrometers can currently be purchased [13], [14]; however, these only serve as detectors and must be paired with accompanying light sources, sample holders and optics in order to be used in the context of testing. Groups have successfully demonstrated portable and compact all-in-one testing platforms, using them to run chemical and biological assays [8], [15], [16]. Due to their ubiquity, and constantly improving hardware and software, smartphones are a favorable candidate for integration with spectroscopic technologies. Interest in smartphone-based technology has grown in lock step with the increasing popularity of the devices. Several groups have designed analysis tools around current generation smartphones, taking advantage of their built-in light sources and image sensors to perform absorption and fluorescence assays [15], [8]. In the aforementioned works, the systems are designed around the smartphones, which serve as light sources and detectors.

In this work, a smartphone biosensing platform is presented, with the goal to be directly integrated into next-generation smartphones. With this goal in mind, a system is proposed that is designed around a CMOS image sensor, commonly used in smartphones, instead of the smartphone itself. This work presents the design, fabrication and characterization of compact measurement platforms capable of both absorption and fluorescence spectroscopic analysis using linear variable filters (LVFs), which are optical components that behave as spatially dependent bandpass filters, separating incoming light into its wavelength-based spectrum. LVFs achieve results similar to those of diffraction gratings, without the need for long optical path lengths to ensure high resolution. Combining such a filter with a conventional CMOS image sensor allows for a compact detection platform to be envisioned.

Work in this space has previously been undertaken, resulting in LVF-enabled detection tools capable of performing spectroscopic measurements in the UV [17], visible [18] and the IR regimes [19], and employed for measuring gas composition [20]. Absorption and fluorescence spectroscopy are particularly of interest as they represent relatively simple techniques that are utilized across a wide range of chemical and biological assays. This work proposes LVF-based spectroscopic systems capable of performing absorption and fluorescence spectroscopy with a footprint within the same order of magnitude as the CMOS sensor. An LVF-based benchtop detection setup is initially presented followed by its miniaturized successors: compact absorption and fluorescence detection platforms. A series of tests is discussed, most notably an enzyme-linked immunosorbent assay used to measure concentrations of human fetal fibronectin, a predictor of preterm birth, as a real-world contextualization of the absorption platform.

1.2 Background

In this section, a theoretical overview of the mechanisms and principles governing the operation of the proposed biosensing system is conducted. This overview serves to accompany the experimental work presented in this work and acts as a reference to better understand the operation of the LVF-based platform.

1.2.1 Fabry-Perot Interferometer

In order to effectively discuss the linear variable filter, single wavelength
Fabry-Perot (FP) interferometers are first presented. By engineering proper-
ties such as cavity length, and index of refraction, these are used to produce
bandpass transmission filters tuned around desired wavelengths. FP-based
optical filters operate on the principle of cavity resonance. Resonant cavi-
ties are cavities bounded by mirrors with specific parameters that impose a
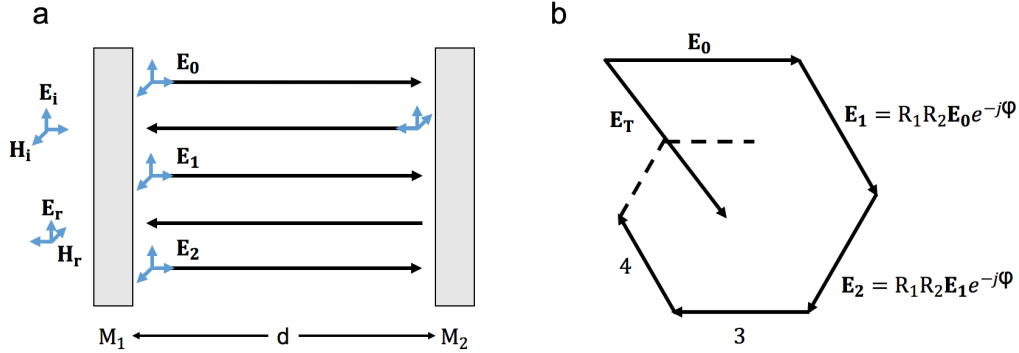resonant wavelength on the system.

Figure 1.1: *(a) Generic optical cavity. (b) Phasor diagram. (Adapted from
[21])*

In order to properly illustrate this phenomenon, a derivation is presented
from an electromagnetics point of view [21]. In order to simplify calculations,
normal incident plane waves are considered. For a general derivation, the
reader can refer to Silfvast's *Laser Fundamentals* [22]. Consider a plane
wave, $\mathbf{E_0}$, reflecting back and forth in an optical cavity, shown in Figure 1.1
(a). Let M_1 and M_2 be mirrors bounding the cavity, with R_1 and R_2 being
their respective reflectivities. After propagating to the M_2 and back, the
wave becomes $\mathbf{E_1} = R_1 R_2 \mathbf{E_0} e^{-jk2d}$, with an added phase term e^{-jk2d} [21].
This is called the round trip phase shift (RTPS), also written 2θ defined as:

$$2\theta = 2kd = q2\pi - \phi, \tag{1.1}$$

where $k = \omega n/c$ is the propagation constant, d is the cavity length, q is an
integer and ϕ the deficiency causing a phase lag [21]. The wave bounces back
and forth ad infinitum, resulting in a total wave $\mathbf{E_T} = \mathbf{E_0}\mathbf{E_1}\mathbf{E_2}$.... Figure 1.1
(b) illustrates the influence of a large ϕ. The resulting wave E_T will have a

3

significantly larger amplitude as ϕ goes to 0. This is called resonance, where:

$$\text{RTPS} = 2kd = q2\pi. \tag{1.2}$$

Substituting $k = \omega n/c = 2\pi/\lambda$ into the RTPS relationship, we obtain a relationship between cavity length and resonant wavelength.

$$d = \frac{q\lambda}{2}, \tag{1.3}$$

where $\lambda = \lambda_0/n$. This equation sums up the resonant condition fairly well. The cavity length needs to be an integer number of half-wavelengths in order to produce resonance at that wavelength [21].

When designing an FP bandpass filter, a cavity is sandwiched between two mirrors with high reflectivities. In practice, distributed Bragg gratings are used as the mirrors, offering high reflectivity, while the cavity is commonly a single dielectric layer, tuned for a specific wavelength. DBRs are alternating stacks of dielectric with contrasting indexes of refraction producing a stop band response around a given wavelength [23]. Figure 1.2 (a) shows the response of a generic DBR stack, showcasing its high reflectivity around the wavelength of interest. Figure 1.2 (b) shows the layer structure of a generic FP optical filter. Light incident onto the surface of the filter is only transmitted if it meets the cavity's resonant condition.
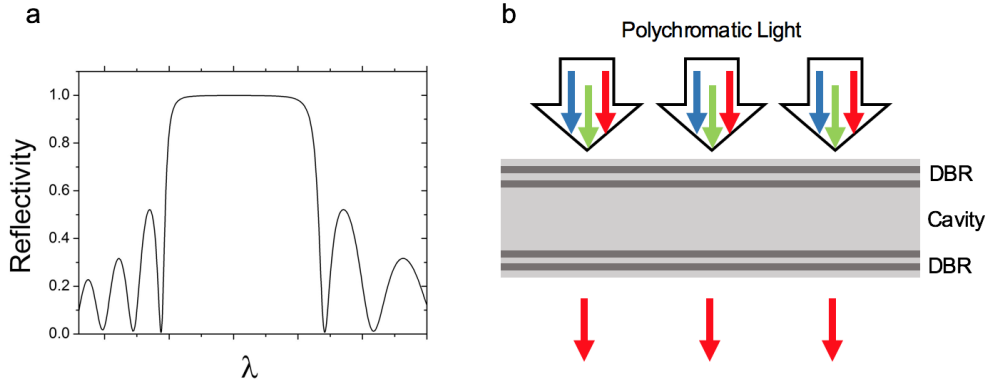

Figure 1.2: *(a) Reflectivity of a DBR structure versus wavelength. (b) Generic FP filter.*

1.2.2 Linear Variable Filter

The linear variable filter (LVF) forms the basis of the compact spectroscopic systems presented in this work. It behaves as a tapered Fabry-Perot filter, producing a correspondence between transmission wavelength and position. It is analogous to a linear array of discrete FP filters [24], with a wedge separating two DBR stacks, acting as mirrors. The wedge is a graded optical cavity bounded by the two dielectric mirrors, resulting in linearly increasing transmission wavelengths along the length of the optical filter. Figure 1.3 illustrates the operating principle of the LVF. Consider a polychromatic light incident onto an LVF operating in the visible regime. This light will only be partially transmitted by the portion of the LVF whose cavity length induces a resonant transmission peak at a specific wavelength. This results in the transmission of different-wavelength light at different spatial positions on the filter. This position-dependent transmission allows for incident light to be transformed into a corresponding wavelength-dependent intensity profile.
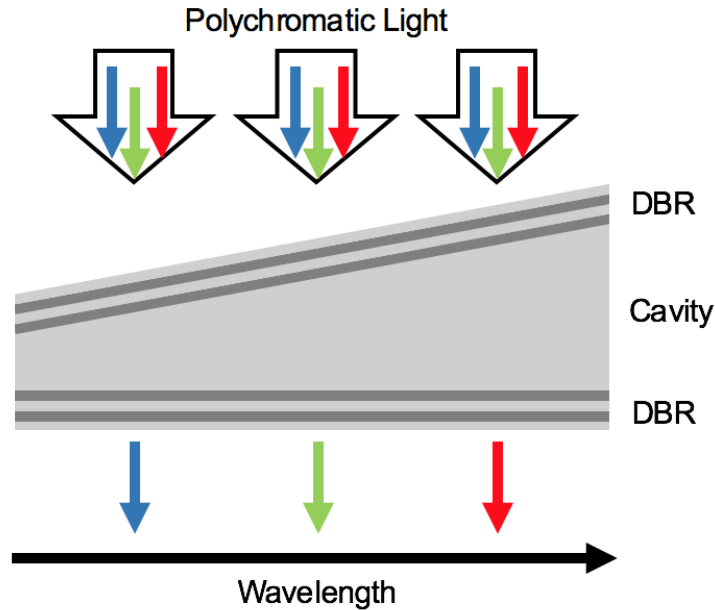
Figure 1.3: *LVF principle of operation.*

Fabrication of the LVF relies on the deposition of a graded wedge separating the dielectric stacks. The taper has been successfully generated using different methods. In 1998, a method was proposed by Seddon et al. [25] to fabricate the LVF. The technique combines radially variable filter fabrication

methods with ion-assisted deposition in order to produce a radially variable filter. Slices are cut from the resulting substrate, producing the LVFs.

In 2009, Emadi et al. [24] proposed an alternative method to fabricate LVFs. In order to achieve the graded cavity layer, photoresist (PR) is first spun onto the wafer. Lithography is then performed, patterning stripes into the PR at decreasing increments of distance. The PR is then heated and reflowed, resulting in a graded slope. The angle of the graded layer can be engineered via the patterning of the PR [24]. The PR layer is then transferred onto the SiO_2 layer via a resistive ion etch, producing a sloped cavity layer. The final DBR stack can then be deposited on top of the cavity layer, producing the LVF [24].

1.2.3   Absorption

Throughout this work, compact spectroscopic systems are demonstrated and characterized via a series of absorption and fluorescence spectroscopy tests. A brief discussion on absorption and fluorescence is presented here in order to properly illustrate the underlying mechanisms behind the proposed detection platforms.

Samples and materials exhibit absorptive properties in certain regions of the wavelength spectrum. Glass, for example, is transparent in the visible region and absorptive in the UV and IR regimes. This phenomenon rests at the heart of spectrophotometry, defined as the quantitative measurement of the scattering and absorption properties of a given sample. For example, spectrophotometry can be used to calculate the concentration of a biological or chemical analyte, labeled by a colored dye.

In this work, sample absorbances are compared in the context of colorimetric tests. By measuring the absorbance of colored samples, analyte concentration can effectively be measured. By comparing the intensity of the transmitted light through a sample P, and to the intensity of the incident light P_0, the transmittance through a given sample can be calculated as $T = P/P_0$. Transmittance is then converted to absorbance via the following relationship [26]: $A = log_{10}P_0/P$, where A is the absorbance of a given sample. The concentration of the absorbing analyte can then be computed using the Beer-Lambert law: $A = a * b * c$, where a is the (usually known)

wavelength-dependent absorptivity coefficient, b, the sample path length, and c, the analyte's concentration [26].

1.2.4 Fluorescence

In the previous section, absorption was briefly discussed. However, the fate of the absorbed light was not touched upon. While the energy of the absorbed light can be dissipated via non-radiative or vibration-related mechanisms, in some cases, it can be re-emitted as light. This is called fluorescence. Fluorescent molecules are best described as multi-level systems consisting of a ground state, S_0, and an excited state, S_1, separated by a transition energy ΔE [27], as shown in Figure 1.4. Polyatomic molecules in a solution possess many vibrational and rotational sublevels that effectively spread the ground and excited states into bands, resulting in a range of possible excitation and emission wavelengths for a given fluorescent molecule [27].
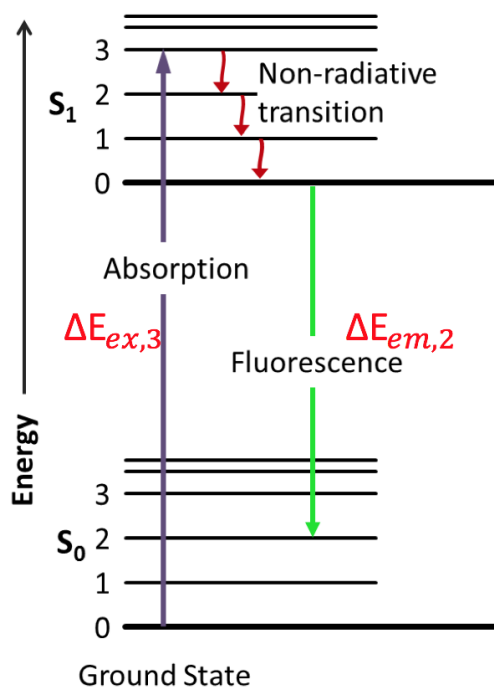

Figure 1.4: *Jablonski diagram illustrating fluorescence.*

When light is absorbed by the molecule with a frequency $v_{ex,i}$ such that $hv_{ex,i} = \Delta E_{ex,i}$, the molecule is excited to $S_{1,i}$, one of the subbands of the excited state. It remains in this state for a short time (1-10 ns) before relaxing

to $S_{1,0}$ [28]. This transition is caused by interactions between the molecule and its solvent environment and is non-radiative [27]. From $S_{1,0}$, a photon of energy $\Delta E_{em,j} = h v_{em,j}$ is emitted with $S_{0,j}$ being a ground state subband. Since $\Delta E_{em,j} < \Delta E_{ex,i}$, the emitted light exhibits a longer wavelength. The difference between energies $h v_{ex,i} - h v_{em,j}$ is called the Stokes shift [28].

1.3   Overview

This work is organized into chapters illustrating the evolution of a compact LVF-enabled spectrometer. Chapter 2 covers the characterization of an LVF-on-CMOS detector, tested via a series of benchtop absorption and fluorescence experiments. These initial experiments serve as a proof-of-concept demonstrating the spectroscopic potential of an LVF-based spectrometer as well as comparing the LVF detector to conventional spectroscopic equipment. Chapter 3 covers the design and fabrication of a miniaturized LVF-based biosensing system for absorption spectroscopy, representing a step in the direction of smartphone integration. Additionally, accompanying experiments are presented and the system's limitations are discussed. In Chapter 4, the design and fabrication of a fluorescence spectroscopy version of the platform discussed in Chapter 3 are covered and preliminary results are reported.

The experiments were carried out in the optical labs of both Prof. Cunningham and Prof. Dallesasse.

CHAPTER 2

BENCH-TOP SYSTEM

2.1 Overview

Before an integrated solution can be proposed, a benchtop LVF-enabled spec-
troscopic system has to be designed and tested. The first iteration of the
compact spectroscopic system consists of two LVFs (JDS Uniphase Corpora-
tion) affixed atop a CMOS image sensor (PixeLINK). CMOS image sensors
are commonly used in current-generation smartphones. By combining them
with LVFs, a spectroscopic system with potential mobile integration can be
effectively demonstrated. These filters act as a continuous series of trans-
mission filters covering a range of wavelengths. This configuration results in
a system capable of detecting spectroscopic signals ranging from 400 nm to
1080 nm. By shining a light emitter at the LVFs, light is spatially separated
by wavelength and filtered onto the CMOS sensor. Figure 2.1 illustrates this
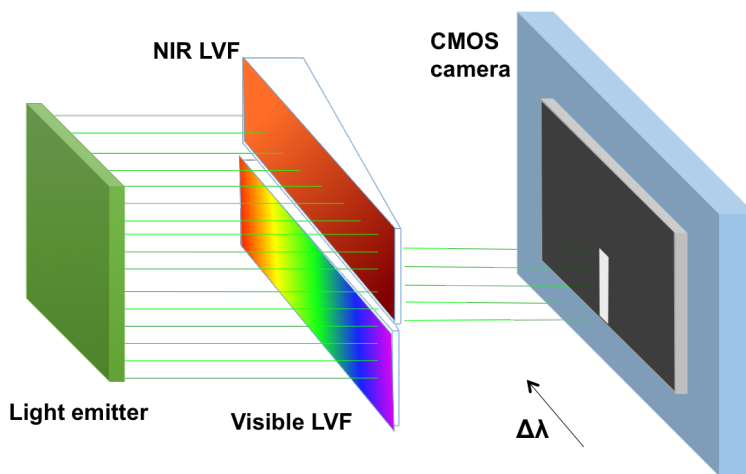process.

Figure 2.1: *Basic operating principle of the LVF-based system.*

An image is obtained using image capture software (*PixeLINK*). The soft-

ware allows the user to specify a series of capture properties, such as exposure time and brightness. Figure 2.2 (Left) shows a standard image obtained while shining a light source on the LVF-CMOS system. The black rectangular bars show the VIS and NIR LVFs, covering their respective portions of the CMOS sensor. Image processing is done using MATLAB. A portion of the LVF is cropped out and averaged in order to produce a corresponding pixel intensity versus pixel position plot shown in Figure 2.2 (Right). Since the LVF correlates space to wavelength, the pixel number on the x-axis effectively corresponds to a wavelength of light. In this example, the white spot on the visible LVF corresponds to the light from the incident illumination source.
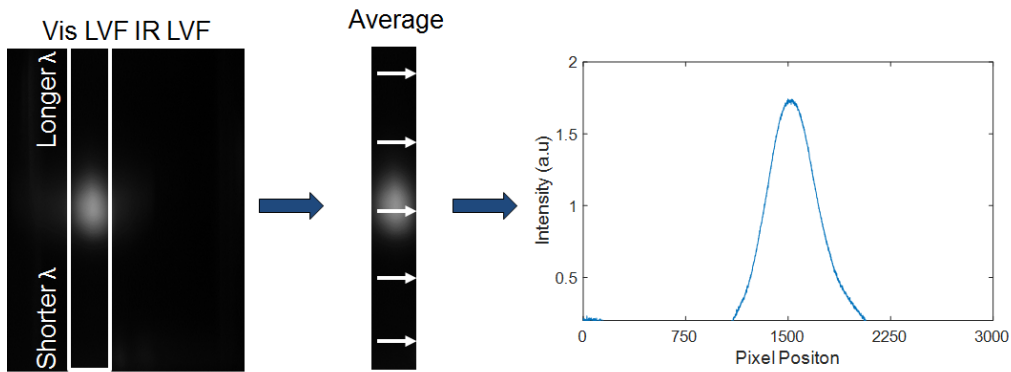

Figure 2.2: *Illustration of the method used to process captured images (Left) into intensity spectra (Right).*

The wavelength values used in the LVF plots are obtained via a pixel to wavelength conversion function. Section 2.6 provides a detailed explanation of how this conversion is derived. Additionally, the CMOS responsivity versus wavelength is taken into account and applied to the gathered data [29].

In order to test the system capabilities in both the absorption and fluorescence modalities, free space optical testing setups are conceived. In the following sections, these setups along with the characteristic experiments undertaken in order to thoroughly test this first iteration of the compact spectroscopic system are presented.

2.2 Absorption Experiments

Figure 2.3 shows the benchtop setup used to gather absorption data. The system is designed to facilitate the simultaneous acquisition of data with the
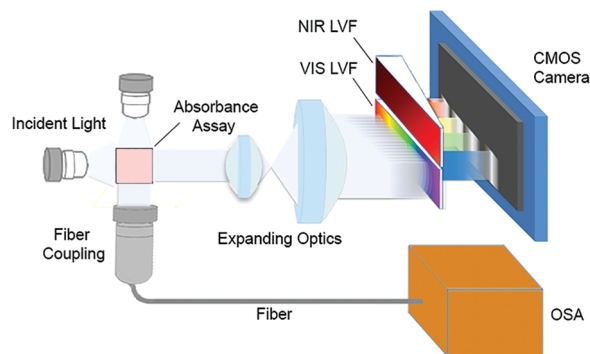
Figure 2.3: *Schematic of benchtop setup used for absorption measurements adapted from [29].*

LVF-on-CMOS system as well as a conventional spectrometer. A sample is introduced to a 3.5 mL quartz cuvette and placed in the beam path of a set of white miniTOPLEDs (OSRAM). The light that is transmitted through the sample can then be simultaneously collected by two detectors: the LVF-on-CMOS and a conventional detector. For the LVF-on-CMOS detector, the transmitted light must be expanded and collimated to cover the entirety of the active region, achieved using a set of optical lenses. Two conventional spectrometers are tested alongside the LVF system: a portable spectrometer (Ocean Optics, USB2000+ VIS-NIR), and an OSA (Yokogawa Electric Corporation, AQ6315B). Light is collected using a standard fiber coupler (SMA to SMA for the portable spectrometer, and SMA to FC/PC for the OSA). This setup allows the user to adequately perform a diverse array of simultaneous absorption experiments, effectively benchmarking the absorption spectroscopy capabilities of the LVF-on-CMOS system.

In the following sections, the experiments are thoroughly presented to illustrate the capabilities of the LVF system compared to conventional spectroscopy equipment. These experiments consist of a measurement of common household food dyes, showcasing the LVF-on-CMOS detector's ability to detect signals over the entire visible wavelength range; a dilution experiment testing the system's ability to differentiate between concentrations of a single solution; and a free chlorine test, as a real-world demonstration of the system's ability to test for the presence of a sample in a solution.

2.2.1   Food Dye Test

Materials and Methods   Several household food dyes (red, orange, green and blue) are dissolved in an aqueous solution and tested. In addition to the red, orange, green, and blue dyes, a white light reference is measured. The samples are then introduced into a series of cuvettes, which are individually placed in the path of an incident white light source. The light transmitted through the sample is collected using the LVF-on-CMOS. It is expanded and collimated onto the LVF and an image is acquired using the accompanying acquisition software (PixeLINK). The images are then processed in MATLAB by the method described in section 2.1. Simultaneously, the transmitted light is collected using both a portable spectrometer and an OSA in order to provide a benchmark for the LVF system.

Once it is gathered, the data is processed and presented as both intensity versus wavelength plots, and transmittance versus wavelength plots. The transmittance data is calculated by dividing each intensity data set by the white light reference data. This allows for a clearer comparison of the detectors, as the idiosyncrasies of each spectroscopy tool are normalized out by the white light reference.

Results   Figure 2.4 shows the resulting data. Plots 2.4 (a, b, c) compare the transmission intensity data gathered by the spectrometer, the OSA, and the LVF respectively. The spectrometer plots show decreased sensitivity in the blue wavelength region when compared to the other two systems. The OSA data looks to be the noisiest of the three. While the OSA boasts higher resolution than the other two systems, thanks to its diffraction gratings and long optical path length, gathered data has to be averaged over multiple measurements in order to limit noise, increasing total measurement time [29]. The LVF system produces data with better SNR than the OSA, comparable to the portable spectrometers [29]. However, fringes can be identified on the intensity plot, resulting in less-than-smooth plots in some wavelength ranges. The fringe effect is believed to be intrinsic to the LVF [29], and potentially a result of the light incident on the LVF being too bright, as the high intensity areas show the most fringes.

Plots 2.4 (d, e, f) show the resulting transmittance plots. These confirm the information gleaned from the intensity plots. For the portable spectrometer,
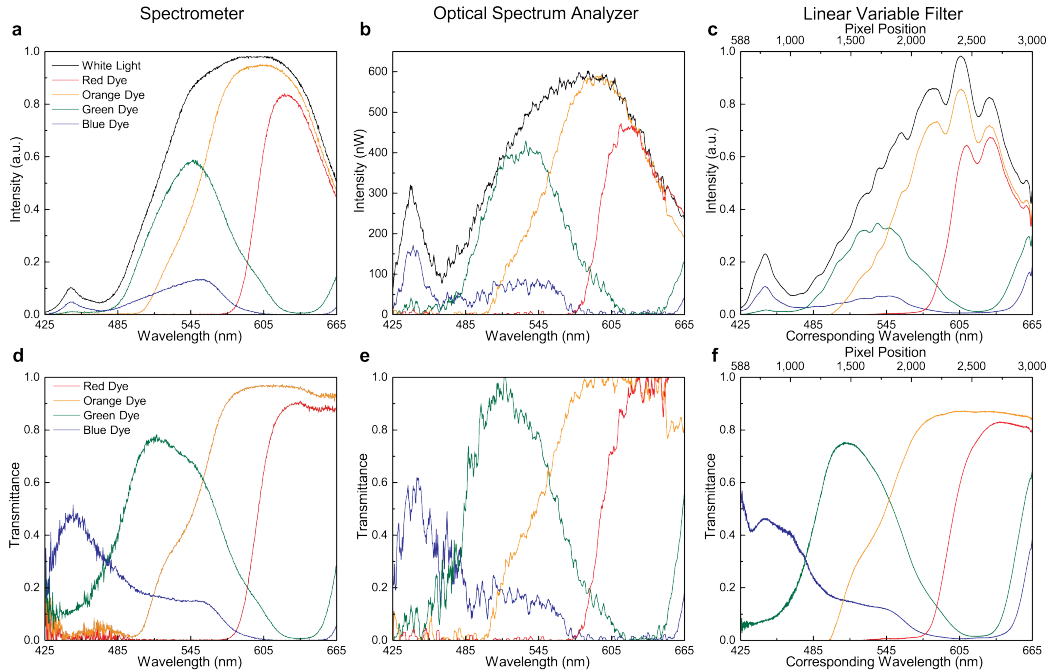
12

Figure 2.4: *Transmission intensities of different food dye samples measured with (a) a portable spectrometer, (b) an OSA, and (c) the LVF system. Corresponding transmittance plots for the (d) portable spectrometer, (e) OSA, and (f) the LVF system [29].*

SNR increases at lower wavelengths, likely due to the CCD's lower sensitivity at these wavelengths [29]. The OSA data is noisy, while the LVF data no longer boasts fringes and has the best SNR across the region of interest.

2.2.2 Dilution Test

Materials and Methods   Four sequential concentrations of green dye solution are prepared and tested using the absorption setup. Each concentration is five times more diluted than the previous one, starting with an arbitrary concentration of dye in an aqueous solution. The samples are tested independently using the LVF-on-CMOS system as well the Ocean Optics spectrometer. The generated intensity and transmittance plots allow for a direct comparison of detector performance. A white light reference image is taken to generate the transmittance plots.
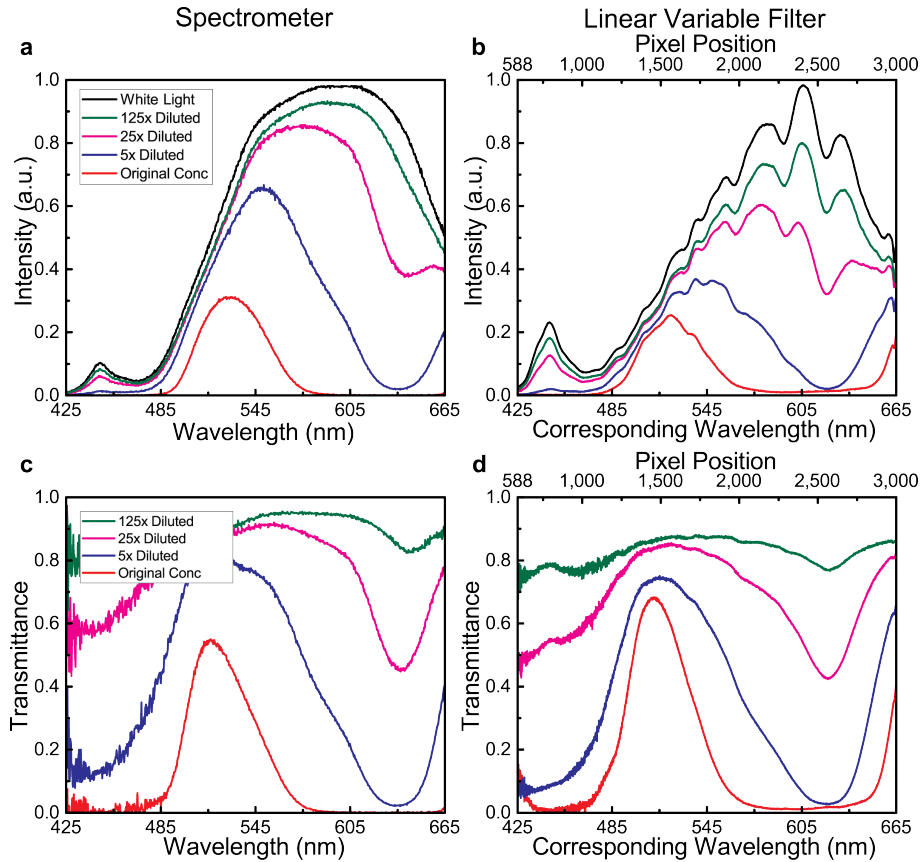
Figure 2.5: *Transmission intensities of different concentrations measured with (a) the portable spectrometer, and (b) the LVF system. Corresponding transmittance plots for (c) the portable spectrometer, and (d) the LVF system [29].*

Results   Figure 2.5 shows the resulting plots. Plots 2.5 (a,b) are intensity versus wavelength plots obtained using the spectrometer and the LVF respectively. As expected, the original concentration results in the weakest signal as the green dye absorbs the white light. Decreasing concentrations result in stronger signals, as confirmed by plots 2.5 (c, d), the resultant transmittance plots. Overall transmission increases as dilutions decrease. The LVF curve shows a clearer response at lower wavelength than the spectrometer counterpart as the spectrometer used is not as sensitive in the blue wavelength region.

2.2.3   Free Chlorine Test

Materials and Methods   In order to subject the LVF system to a real-life measurement, a free chlorine test is performed, representing a commonly used quality measurement for municipal water supplies [30]. A commercially available assay kit is used to test a sample of city tap water (Urbana, IL). DPD (N, N-diethyl-p-phenylenediamine) free chlorine reagent powder pillows (Hach Company) are added to the tap water sample, turning it into a shade of pink. These color the water pink if free chlorine is detected in the sample. A control sample is prepared by DPD pillows to Milli-Q water. Milli-Q water is highly filtered and "ultrapure" water used as a reference sample [29].
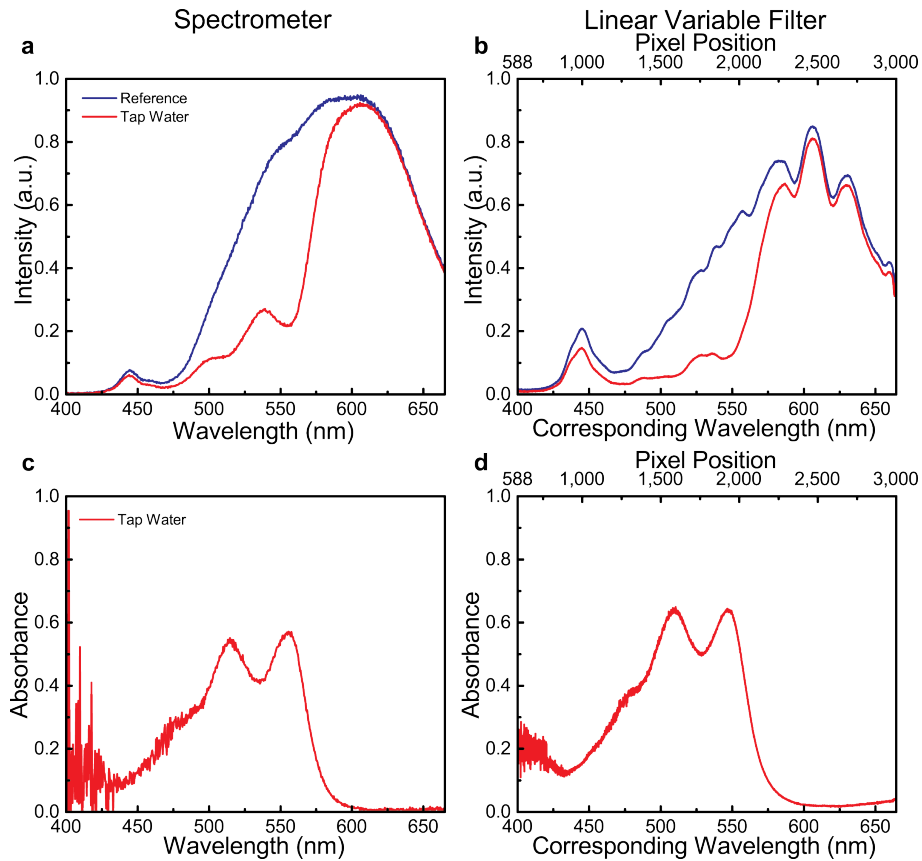

Figure 2.6: *Transmission intensities comparing the Milli-Q water reference and tap water samples measured with (a) the portable spectrometer, and (b) the LVF system. Corresponding absorbance plots for (c) the portable spectrometer, and (d) the LVF system [29].*

Results   Both samples are measured using the LVF-CMOS system as well as the portable spectrometer in order to generate intensity versus wavelength

15

plots shown in Figures 2.6 (a,b). Additionally, absorbance data is calculated from the intensity data. This calculation is done by using the relation discussed previously, $A = log_{10}P_0/P$, where P_0 is the incident light intensity, and P is the transmitted light intensity [29]. Absorbance is plotted in Figures 2.6 (c, d). It is clear that the tap water sample contains chlorine, and this is confirmed by the absorbance plots, which generate a quantitative measurement. Good agreement is observed between the spectrometer and LVF data, further validating the LVF systems colorimetric abilities.
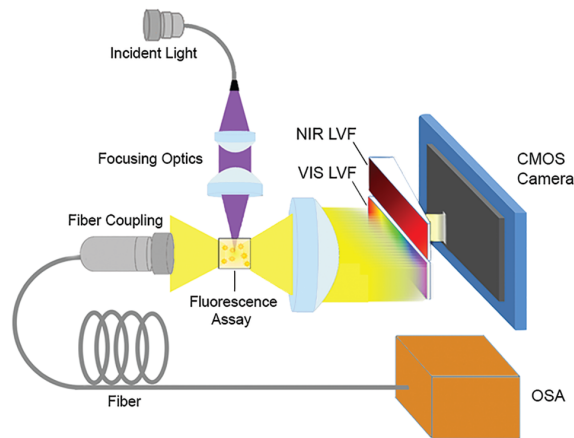
2.3   Fluorescence Experiments

Figure 2.7: *Schematic of benchtop setup used for fluorescence measurements [29].*

Figure 2.7 shows the setup designed for fluorescence experiments. The system is designed to allow for the acquisition of data with both the LVF-on-CMOS system as well as a conventional spectrometer. A quartz cuvette containing the sample to be measured is placed in the path of an incident light. The light excites the fluorophores in the sample which emits isotropically. The emitted light is collected by a collimator, orthogonal to the incident light. This is done to avoid collecting both the fluorescent signal and the much more intense incident light transmitted through the sample [29]. The collected light is then collimated onto the LVF-on-CMOS detector. For the spectrometer, light is collected using an SMA cable. This system allows the user to adequately perform a diverse array of fluorescence experi-

ments, effectively benchmarking the fluorescence spectroscopy capabilities of the LVF-on-CMOS system.

In the following sections, a thorough presentation of the experiments will be made in order to illustrate the capabilities of the system compared to conventional spectroscopy tools. These experiments consist of a comparison of a series fluorescing quantum dyes, showcasing the LVF-on-CMOS detector's ability to detect signals over the entire operating wavelength range, as well as a concentration sweep of a specific fluorophore in order to assess the system's limits of detection.
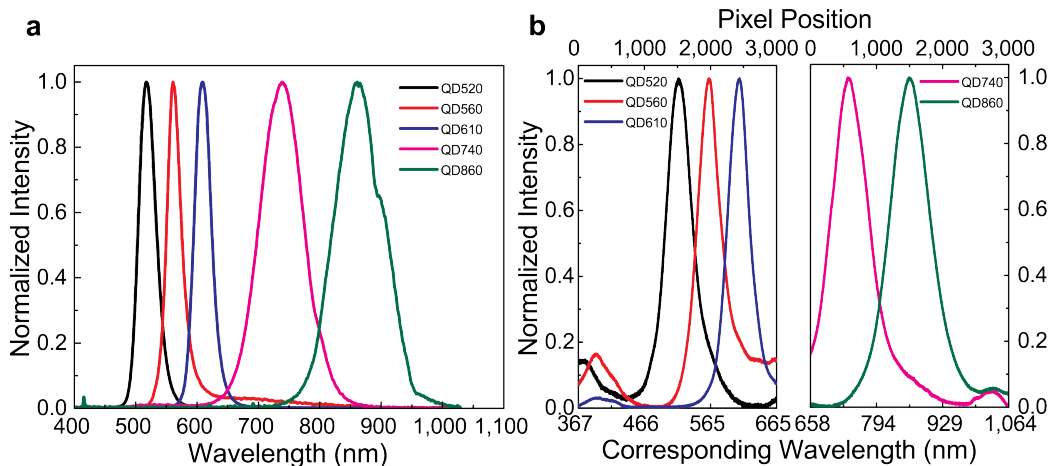
2.3.1   Quantum Dot Test

Figure 2.8: *Fluorescence signals of five QD solutions measured using (a) the portable spectrometer and (b) the LVF system [29].*

Materials and Methods   A series of five QD solutions (QD520, QD560, QD600, QD610, QD740) were prepared in-house by collaborators using a synthesis method reported in their previous works [31], [32]. Additionally, a sixth QD was purchased (QD860-OS). These emit at various peaks across a wavelength regime ranging from 520 nm to 860 nm. These solutions are introduced into quartz cuvettes and sequentially tested using the fluorescence benchtop setup. The incident light in this case is a 410 nm blue laser used to excite the QDs. Both LVF and spectrometer data are collected for each QD sample. The visible QD (520-610 nm) signals are measured using the VIS-

LVF, while the higher emission wavelength QD signals are measured using the NIR-LVF.

Results Figure 2.8 shows QD measurements using both the LVF system and a conventional spectrometer. The LVF data is split across two plots (VIS and NIR) and plotted versus both pixel and corresponding wavelength. The plots show good agreement between both detection systems, demonstrating the system's ability to measure signals across a wide wavelength range.

2.3.2 Dilution Test

Materials and Methods Two sets of dilution experiments are prepared using QD600 and near-infrared dye 800CW carboxylate (IRdye) solutions. Data is collected exclusively by the LVF-CMOS as this experiment serves to determine the system's limit of detection. Beginning with the stock concentrations (760nM for the QD600, and 20ug/mL for the IRdye), each sample undergoes a series of five-fold dilutions. Both sets of samples are then tested using the fluorescence setup. Three separate tests are undertaken for each sample set. The QD600 samples are excited with a 410 nm blue laser, while the IRdye samples are excited using a 785 nm laser (Ocean Optics). Images are captured using the PixeLINK image capture software. As the concentration decreases between each sample, exposure time is increased in order to resolve the signal. As such, the final results are normalized by the exposure time used during the capture during post-processing. For the QD600 measurements, the lowest exposure time used was 2000 ms for the 0.28 nM sample [29]. Additionally, the QD600 data was processed from the VIS LVF portion of the CMOS, while the IRdye data was generated from the NIR LVF region of interest.

Results Figures 2.9 (a,c) show the resulting intensity versus wavelength plots for the QD600 and IRdye samples respectively. As expected, lower concentrations result in lower intensity spectra. Concentrations as low as 0.28 nM (VIS LVF) and 32 ng/mL (IR LVF) are successfully resolved by the system, as can be seen in the insets. The intensity plots are integrated and plotted versus concentration in Figures 2.9 (b, d) showing a clear increase in intensity as concentration increases. This set of experiments prompts a
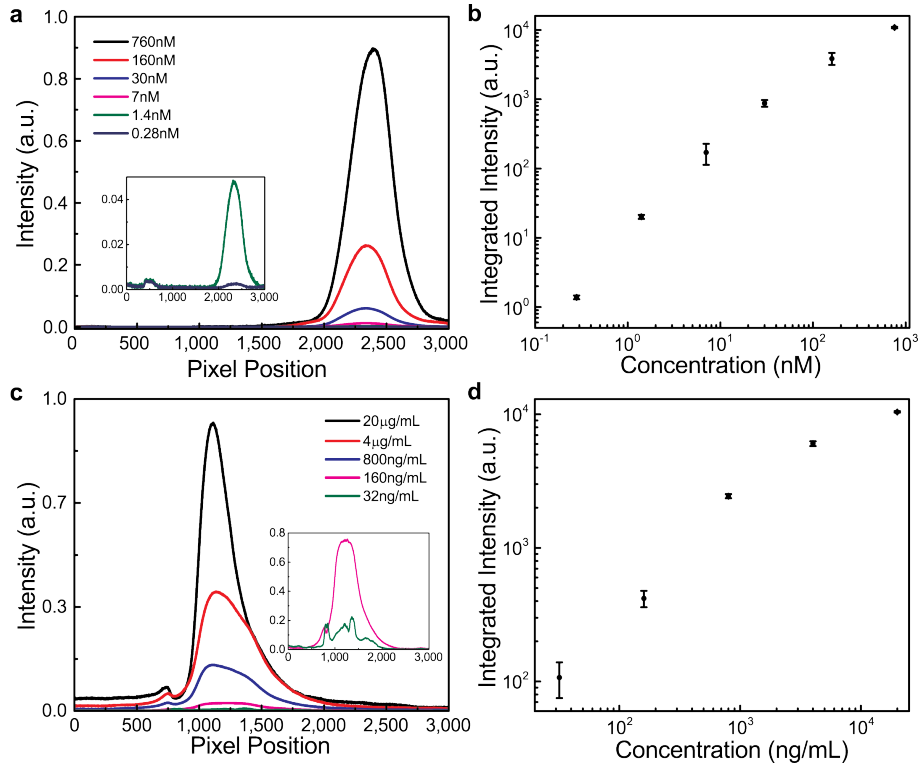
Figure 2.9: *Fluorescence intensity plots of sets of five-fold dilutions of (a) QD600 solutions, and (c) IRdye solutions. Whisker plots of integrated intensity plotted versus concentration for the (b) QD600 solutions and the (d) IRdye solutions [29].*

discussion of the system's limits of detection in both the visible and NIR regimes.

2.4   Spatial-Spectral Conversion

In order to accurately undertake a series of benchmark experiments, the LVFs first have to be thoroughly characterized. An accurate pixel-position-to-wavelength conversion must be determined in order to better make sense of the generated data. This conversion is obtained by comparing data obtained with the LVF (intensity versus pixel position), with data obtained using the spectrometer and the OSA (intensity versus wavelength) in order to generate a linear relationship between pixel position and wavelength.
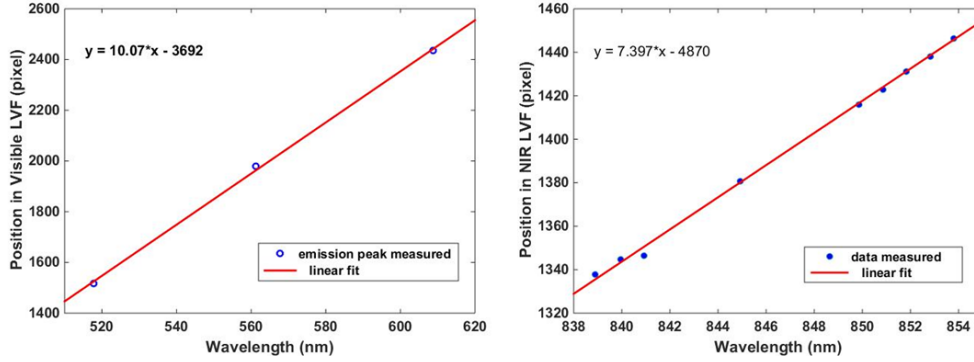
19

Figure 2.10: *Pixel-wavelength conversion plot for (a) the VIS LVF, and (b) the NIR LVF.*

2.4.1 Visible LVF

Materials and Methods In order to derive a conversion function for the visible LVF across its operating wavelength (400-800 nm), data from the visible QD experiment by the LVF and the portable spectrometer is used. The locations of the emission maxima are plotted against each other and a linear fit is made using MATLAB.

Results Figure 2.10 (a) shows the resulting pixel versus wavelength relation. The resulting conversion function is:

$$x_{px} = 10.07 * \lambda - 3692, \tag{2.1}$$

where x_{px} is pixel position and λ is wavelength.

It is found that every nanometer in the wavelength domain corresponds to a separation of 10.07 pixels. An estimation of the LVF resolution can then be calculated, coming out to 3.77 nm.

2.4.2 Near-IR LVF

Materials and Methods A tunable infrared laser (New Focus 6300) capable of emitting single wavelengths from 838 nm to 856 nm is used to determine the pixel-to-wavelength correlation for the NIR-LVF. Data is gathered at 1 nm steps swept across the laser's operating wavelength using the LVF system, the portable spectrometer and the OSA. The wavelength peak locations

are then plotted against each other and a linear fit is made.

Results   Figure 2.10b shows the resulting pixel versus wavelength relation. The resulting conversion function is:

$$x_{px} = 7.397 * \lambda - 4870, \tag{2.2}$$

where x_{px} is pixel position and λ is wavelength.

It is found that every nanometer in the wavelength domain corresponds to a separation of 7.4 pixels. An estimation of the LVF resolution can then be calculated, coming out to 6.09 nm.

2.5   Summary of Results

In this chapter, the inception and characterization of a compact spectroscopic system are presented. The system is tested in both absorption and fluorescence modalities, via dedicated benchtop characterization setups, utilizing free-space optics and external illumination sources. By way of various colorimetric and fluorometry experiments, the LVF system is tested against both a portable spectrometer and an OSA, showing good agreement with both conventional spectroscopy tools. Three dilution experiments are undertaken in order to estimate the system's detection limits in both the absorption and fluorescence modalities. Calibration experiments are run to determine a pixel-wavelength conversion ratio, and the resolution of each LVF is estimated. These experiments effectively illustrate the abilities of the LVF-on-CMOS system as a spectrometer. This benchmarking phase represents a first step towards the ultimate goal of developing an all-encompassing integrated sensing platform.

CHAPTER 3

ABSORPTION PLATFORM

3.1 Overview

Building on the success of the benchtop experiments, a compact system represents the next milestone, aiming to package the components of the benchtop setups around the CMOS sensor in order to minimize the system's overall footprint, while retaining its original functionality. The compact platform is designed with the intent of ultimately integrating it with a next-generation smartphone. As such, compactness and versatility are of great importance. While the ultimate goal of the project is to develop a system capable of both absorption and fluorescence spectroscopy using a single CMOS sensor, separate platforms are designed and fabricated in order to test both modalities individually and facilitate troubleshooting.

In this chapter, the absorption platform is presented, along with the series of experiments performed to characterize it showcasing its colorimetric ability. The absorption platform combines a VIS LVF bonded atop a CMOS image sensor (Framos, GCPM1931), three white miniTOPLEDS (OSRAM), a collimating rod lens, and a sample-holding apparatus consisting of a holding base and a detachable microfluidic cartridge, providing a compact alternative to the benchtop experimental setup. These components are configured to endow the system with the ability to perform absorption assays without the use of external optics and light sources.

Using the absorption platform, samples can be measured in a handful of steps. First, the system must be properly connected to both a current source via leads soldered onto the LED PCB shown in Figure 3.1 (b) and the computer used to capture data via an Ethernet cable attached to the CMOS sensor system. The current source is used to drive the LEDs at 20 mA, replacing a smartphone built-in power source. Once the system is connected,

the sample must be introduced into the fluidic channel of the sample cartridge used. For absorption measurement, the sample cartridges used must have a mirror on the backside of each fluidic channel. The cartridge is then snapped onto the holding base and the current source is turned on. Light transmitted into the sample reflects off of the mirror coating the backside of the fluidic channel and is collected by the LVF-covered CMOS detector, providing information on the absorption of the measured sample. Images can then be captured using the GigE vision image capture software. Similar to the benchtop experiments, exposure time and brightness can be controlled when capturing images. The images are then processed with MATLAB using the method described in section 2.1, making sure to account for the new camera's responsivity across the operating wavelength region.

In the following sections, the absorption platform is presented. Its design specifications are discussed at length, and the experiments carried out to test it are presented. The experiments are designed to showcase the platform's ability to test liquid-phase samples, particularly in the context of an ELISA assay. Additionally, its potential to perform solid-phase sample tests is explored and discussed via a series of characteristic experiments.

3.2   System Design

Figure 3.1 shows a detailed schematic of the proposed system. The design can be broken down into three major parts: the LVF-CMOS camera detector, illumination and optics, and the sample holder. In this section, the design steps involved in the fabrication of each of these components are described.

3.2.1   Image Sensor and LVF

The placement of the LVF on the CMOS sensor represents the key innovation that enables the system's functionality as a compact spectroscopy tool. While it is simply taped onto the surface of the CMOS sensor in the benchtop version, the LVF must be permanently affixed on the CMOS sensor in order to ensure reproducible data and portability. This is accomplished by bonding the LVF onto the sensor using a UV curable epoxy.

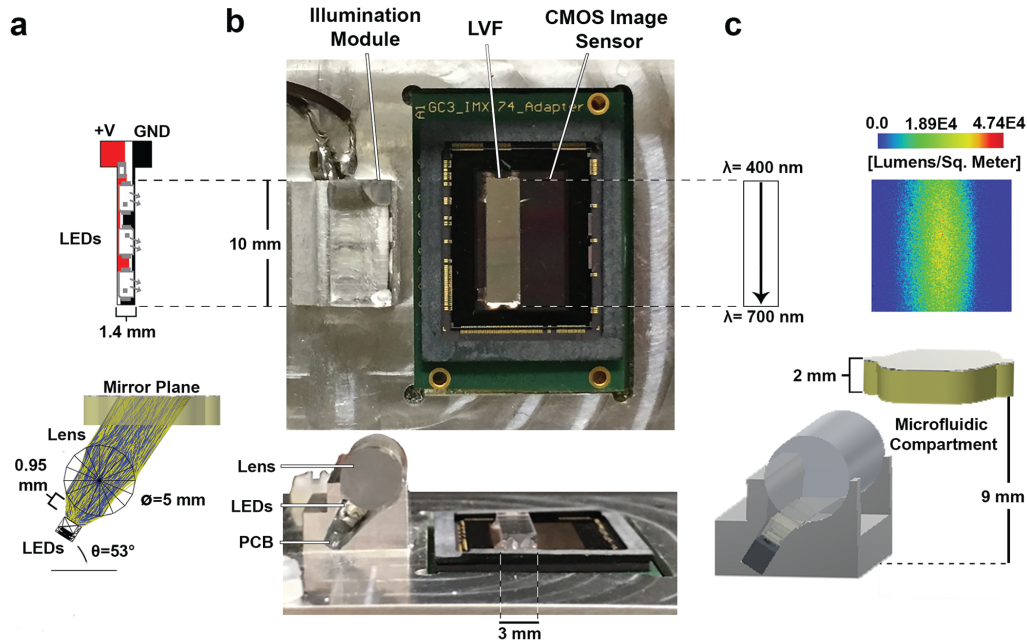The VIS LVF is longer than the active region of the CMOS sensor. In order

Figure 3.1: *(a) Schematics of the PCB design and collimating lens setup for the LED illumination module. (b) Front-view and top-view photographs of the integrated system. (c) Simulated output of the intensity distribution from the collimated light source measured at the plane of the mirror within the microfluidic compartment (adapted from [33]).*

to properly bond it onto the CMOS, it must be diced down to a smaller size. In order to ensure that the parts of the filter that are diced off lie outside of the wavelength regime required for the planned experiments, the LVF is characterized using a spectrophotometer (Varian Cary 5 G). This allows for a safe portion of the LVF to be marked for dicing.

Before dicing the LVF, it is first affixed to a silicon substrate using thermally activated paraffin wax and spin-coated with a layer of photoresist (S1813). The resultant stack is then diced with the Disco DAD-6TM wafer dicing saw and a shortened LVF can be recovered. The LVF is then placed on top of the CMOS sensor and held in place via single drops of UV-curable epoxy (NEA 123) dispensed using a precision fluid dispensing system (EFD, Nordson). The epoxy is cured for over 30 seconds using a standard UV lamp (Xenon).

3.2.2 Illumination and Optics

Three white miniTOPLEDs (OSRAM) with a broadband spectrum extending from 400 to 800 nm, act as the system's illumination source. These are soldered along with a resistor onto a PCB. The LEDs are diverging sources which need to be collimated in order to achieve accurate absorption measurement. A rod lens sitting between the LEDs and the sample channel is used to collimate the incident signal.

The spatial configuration of the illumination sources, the rod lens and the LVF is determined using Zemax OpticStudio models shown in Figure 3.1 (a). Zemax is an optical design ray tracing software suite. In order to successfully make a measurement, the LED light must be collimated by the rod lens, transmitted through the sample, and reflected by the mirror coating the back of the channel onto the LVF-covered CMOS sensor. Zemax is used to determine the optimal position of each component in order to ensure that the system performs as desired. Figure 3.1 (c) is an intensity map showing good collimation at the back of the fluidic channel, obtained by moving both the rod lens and the channel, until reasonable collimation is achieved.

Once the spatial position of each component is defined, the Zemax model is imported into standard CAD software (*Inventor*) in order to design a base platform to hold the components in place. Inventor is used to design an aluminum support platform around the individual components. A platform is designed to house the white LEDs and their PCB board, and the rod lens, while sitting around the CMOS image sensor. The fabricated apparatus is then screwed onto the CMOS-sensor chip, effectively surrounding the image sensor as illustrated in Figure 3.1 (b). The PCB and rod lens are bonded to the support platform using UV-curable epoxy.

3.2.3 Sample Holder

The sample holder consists of two separate parts: the holding base and the sample cartridge. Both pieces are designed using conventional CAD software and fabricated stereolithographically (Somos WaterClear Ultra 10122). The holding base is designed to sit around the LVF-CMOS system as shown. The sample cartridge is a detachable component boasting a fluidic channel with two inlet holes allowing for samples to be introduced via a pipette. The

cartridge can be snapped on and off of the holding base, in order to facilitate sample preparation. This also allows for different samples with different fluidic channel volumes to be designed, increasing the system's versatility. In the following experiments, two different types of cartridges are used depending on the nature of the application. One is a standard single-channel cartridge, while the other is an eight-channel cartridge allowing the user to perform multiple tests in quick succession shown in Figure 3.2.

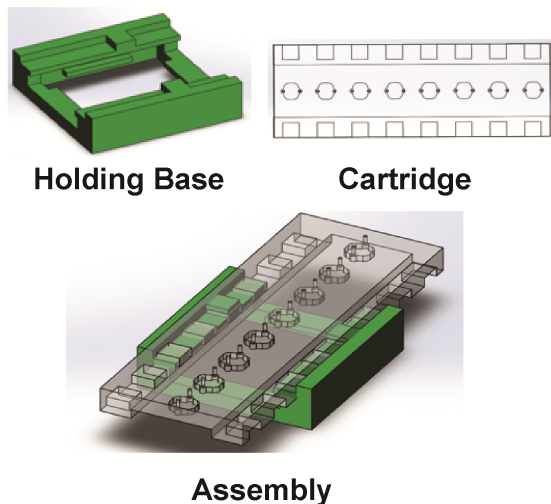**Holding Base**   **Cartridge**

Assembly

Figure 3.2: *Schematic of sample holder and separate components used for multichannel ELISA measurements. (Left) Holding base that sits around the aluminum cage. (Right) Eight-channel cartridge designed for rapid measurements. (Bottom) Combined assembly (adapted from [33]).*

3.3   Experiments

3.3.1   Calibration Experiment

The VIS LVF-CMOS system is characterized to produce pixel-to-wavelength conversion. This is accomplished in a similar manner as described in Chapter 2.5. A series of light sources ($\lambda = 410, 413, 538, 669$ nm) are measured using both the LVF and a portable spectrometer. Additionally, a white light source is used in conjunction with several filters to generate different spectra, measured captured using the LVF system along with the conventional spectrometer.

The resulting LVF and spectrometer intensity data sets are plotted in Figures 3.3 (a), and 3.3 (b) respectively. The characteristic points of each spectrum are extracted from both sets of data. These are plotted against each other in order to generate a pixel-to-wavelength conversion shown in Figure 3.3 (c).
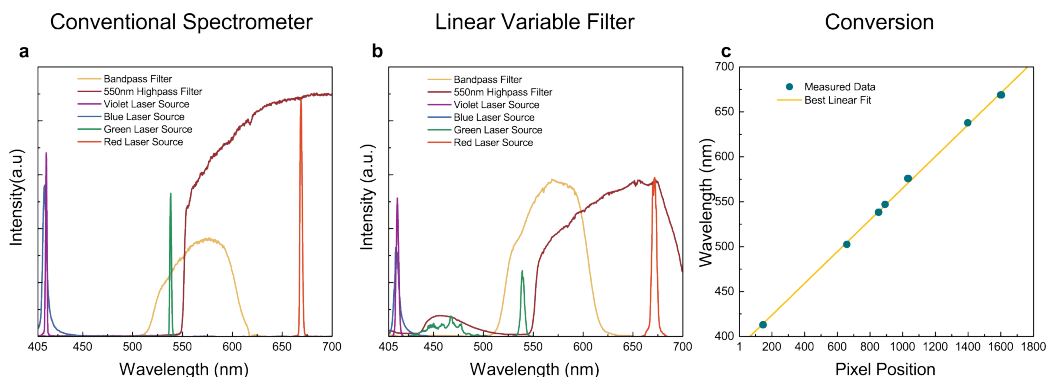

Figure 3.3: *Spectra of various laser sources and filtered white light measured with (a) a conventional spectrometer and (b) the compact LVF spectrometer system. (c) The resulting pixel-to-wavelength conversion for the LVF spectrometer [33].*

3.3.2 Food Dye Test

Materials and Methods Blue, green, and red food dyes are dissolved in water in order to verify the system's colorimetric capabilities. Before the samples are tested, a water measurement is taken as a reference. The samples are inserted into the sample cartridge channels via the inlets using a pipette.

Results Figure 3.4 (a) shows the images captured using the GigE Vision software for the white light, red, blue and green dyes. Only the LVFs active area is shown. Sections of the white bands visible on the white light reference image can be seen across the rest of the sample images. The colored solutions are absorbing the incident light at different wavelength regions. Figures 3.4 (b) and 3.4 (c) clearly demonstrate this, as each solution transmits a wavelength regime that correlates with its color. These results confirm the system's colorimetric capabilities across the visible wavelength regime.
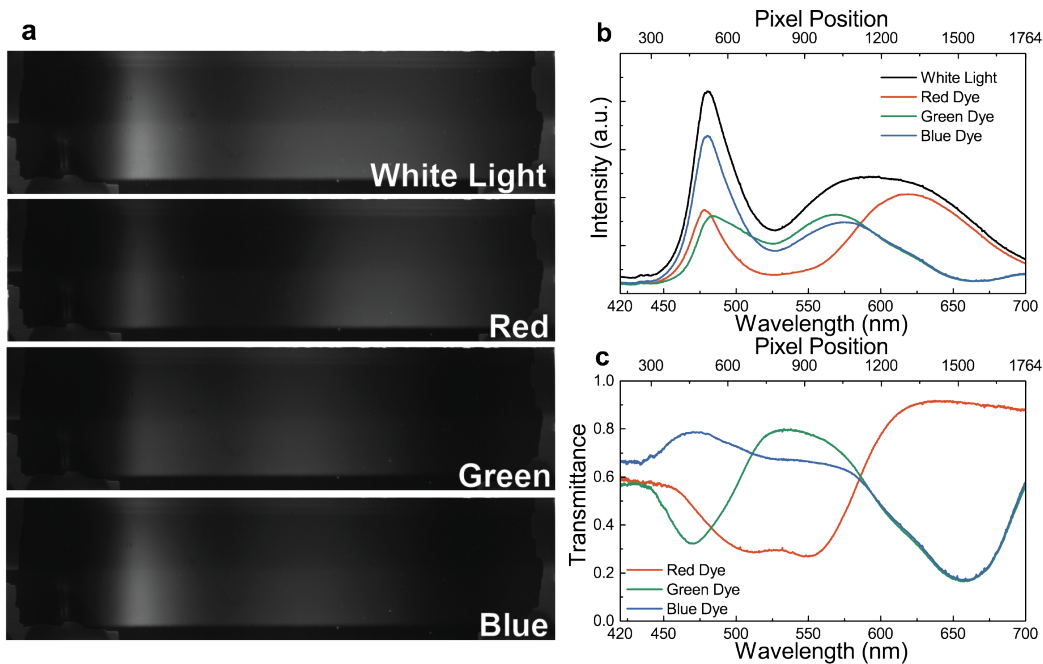
Figure 3.4: *(a) Images from the LVF-covered CMOS image sensor obtained during household food dye measurements. (b) Processed intensity plots for each measured sample. (c) Transmittance plots obtained after normalizing by the white light reference [33].*

3.3.3 Enzyme-Linked Immunosorbent Assay

Materials and Methods   A commercially available ELISA kit (CUSABIO) for the quantification of human fetal fibronectin (fFN) is prepared. ELISA is used to quantify analytes in samples via absorption tests. Samples are prepared by immobilizing the biomolecule of interest onto the surface of a well using analyte-specific antibodies and antigens labeled with an enzyme [34]. The surface is washed with a series of liquids to do away with unbound substances. A solution containing the substrate matching the enzyme is then added to the well, producing a change of color, which can be measured and used to determine the concentration of the biomolecule in the sample [34]. The analyte's concentration is determined by comparing the measured absorbance to a calibration curve obtained by measuring a series of known standards. In this work, the LVF system is used to measure a set of standards for the quantification of human fFN.

Lyophilized fFN is reconstituted in the kit's standard diluent, and serially diluted to six concentrations (1000, 333, 111, 37, 12 and 4 ng/mL). Each sample is pipetted into microplate wells containing an immobilized assay specific

for fFN [35]. A blank well is filled with only diluent buffer. The standards are prepared in triplicate. The assay is then completed per the kit's directions. The plate is read on a 96-well plate reader (BioTek) as soon as the stop solution is added to the wells [33]. The reader measures absorbance at 450 nm. The samples are then pipetted into the fluidic cavities of three separate eight-channel microfluidic cartridges. These are then rapidly tested using the absorption platform. Prior to the sample measurements, each channel is filled with deionized water and measured using the LVF system to provide an adequate reference for absorbance calculations [33].
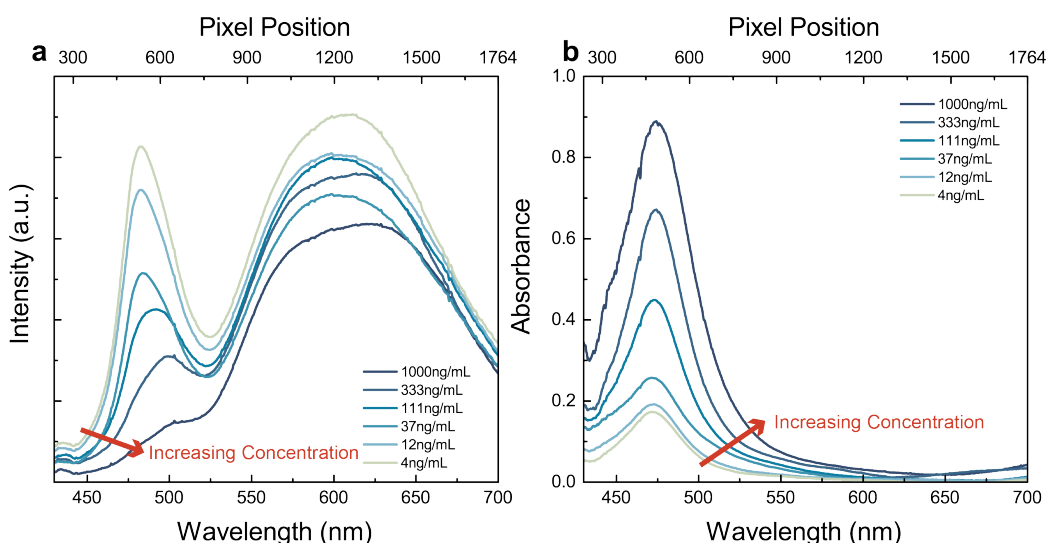

Figure 3.5: *(a) Transmitted intensity spectra of serially diluted fFN ELISA liquid samples measured using the compact LVF system. (b) Absorbance calculated by using the measured water reference data for each sample [33].*

Results The intensity versus wavelength data gathered using the absorption platform is plotted in Figure 3.5 (a). As concentration increases, intensity decreases, particularly in the 450-500 nm region. Absorbance is calculated using the reference data obtained using $A = log_{10}P_0/P$, where P_0 is the incident light intensity, and P is the transmitted light intensity [29]. These plots are shown in Figure 3.5 (b). In order to adequately compare the LVF system to the spectrometer, absorbance versus concentration plots are generated. Figure 3.6 (a) shows the absorbance measured by the microplate reader versus concentration. Since the microplate reader measures absorbance at 450 nm, absorbance data at 450 nm is extracted from the LVF

data and plotted versus concentration, shown in Figure 3.6 (b). Additionally, absorption is integrated from 448 to 510 nm as it is clear that absorption is occurring across a wider regime than just 450 nm. This data is plotted versus concentration in Figure 3.6 (c). A limit of detection value can then be extracted from each plot. This is accomplished by first fitting the data to a four-parameter logistic regression model [35], then plotting a line three standard deviations above zero. The intersection between the plotted line and the fit curve determines the system's limit of detection [8]. This is found to be 4.52 ng/mL for the LVF spectrometer and 8.46 ng/mL for the microplate reader, showing good agreement between both data sets.
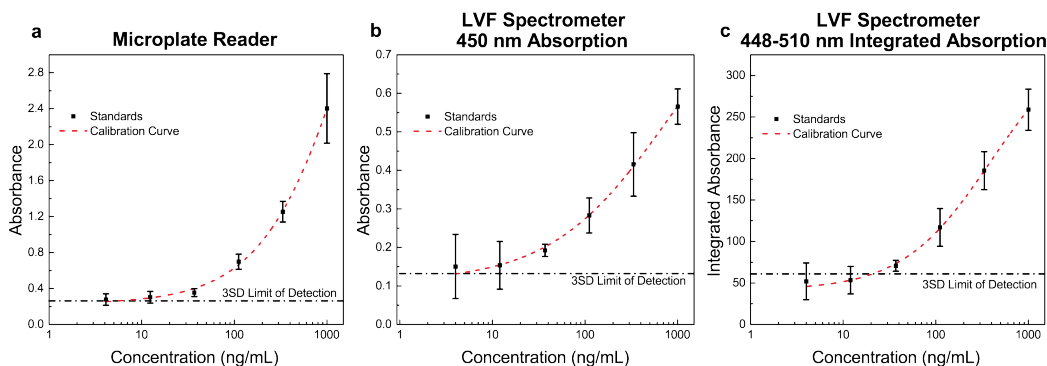

Figure 3.6: *Dose-response absorbance versus concentration plots for the ELISA data measured using (a) microplate reader at 450 nm, the LVF system, (b) only the data at 450 nm, and (c) data integrated from 448 to 510 nm [33].*

3.3.4 Solid-Phase Experiments

Materials and Methods   Two solid-phase experiments are run in order to assess the system's ability to quantify the spectroscopic difference between colored solid objects by measuring scattered spectra. A set of colored Post-It strips are taped onto a mirror-coated microfluidic cartridge and individually tested using the absorption platform. An empty cartridge is also measured to act as a reference. Additionally, pH paper (Hydrion) is used as a testing medium. Strips are exposed to different solutions (water, vinegar, diluted HCl, and baking soda) in order to change their color, and subsequently measured. An empty cartridge measurement is also used as a reference.
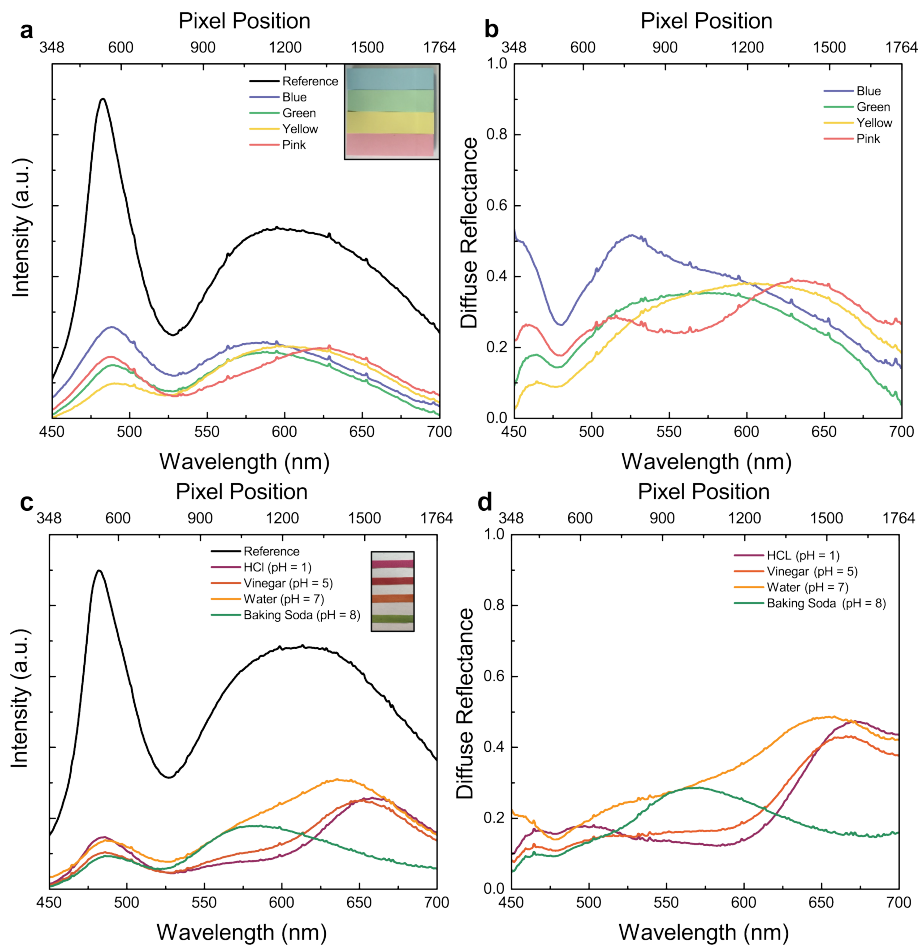
Figure 3.7: *Scattered spectra under white LED illumination of (a) colored sticky notes, and (c) treated pH paper measured with the LVF spectrometer system, including the reference spectra gathered by illuminating a bare mirror-coated microfluidic chamber. Calculated diffuse reflectance for (b) colored sticky notes, and (d) treated pH paper [33].*

Results   Figures 3.7 (a) and 3.7 (b) show the data gathered from the Post-It measurements. The intensity versus wavelength plot shows the differences between the scattered spectra of the different-colored Post-Its. This is confirmed by the calculated diffuse reflectance plot, calculated in the same way as a transmittance plot, with the reflected light divided by the reference. The pH paper test tells a similar story, presented in Figures 3.7 (c), and 3.7 (d). The intensity and diffuse reflectance plots show different scattered spectra between markedly different-colored strips, while showing good agreement between strips of similar color (HCl and Vinegar).

3.4 Summary of Results

In this chapter, the absorption LVF-based platform is discussed. Its design, fabrication and characterization are presented. Through a series of liquid and solid phase experiments, the absorption platform is shown to be a compact, versatile alternative to lab spectrometers. While it cannot compete with laboratory spectrometers in terms of accuracy and efficiency, its footprint and ease of use make it a favorable candidate for point-of-care diagnostics, as evidenced by its ability to successfully run an ELISA assay, with results comparable to a laboratory tool.

CHAPTER 4

FLUORESCENCE PLATFORM

4.1   Overview

While the absorption and fluorescence platforms share certain design characteristics, the idiosyncrasies of fluorescence spectroscopy demand different design considerations. In this chapter, the fluorescence platform is presented, along with the first set of experiments undertaken in order to benchmark the system. The fluorescence platform consists of a NIR LVF bonded atop a CMOS image sensor (Framos, GCPM1931), surrounded by three red mini-TOPLEDS (OSRAM), a focusing rod lens, and a sample holding apparatus consisting of a holding base and a detachable microfluidic cartridge. The NIR LVF is used in conjunction with the red LEDs in order to measure fluorescence signals in the NIR wavelength regime.

Using the fluorescence platform, samples can be measured in a similar manner as with the absorption system. First, the system must be properly connected to both a current source via leads soldered onto the LED PCB and the computer used to capture data via an Ethernet cable attached to the CMOS sensor system. The current source is used to drive the LEDs at 20 mA. Once the system is connected, the sample must be introduced into the fluidic channel of the sample cartridge used. For fluorescence measurement, the sample cartridges do not have a mirror coating the back of the fluidic channel. The reason for this is to limit the amount of incident light reflecting back onto the CMOS sensor in order to avoid drowning out the fluorescence emission signal. The cartridge is then snapped onto the holding base and the current source is turned on. Light focused into the sample excites the fluorophores within, which in turn emit isotropically, shining light onto the LVF-covered CMOS detector. Images can then be captured and processed in the exact same way as is done using the absorption platform.

In the following sections, the fluorescence platform is discussed. Its design specifications are detailed, and the experiments carried out to test it are presented. The initial round of experiments is designed to characterize the system and showcase the platform's ability to successfully measure fluorescence signals.

4.2   System Design

Figure 4.1 shows the fluorescence system in its entirety. The design is broken down into three major parts: the LVF-CMOS camera detector, illumination and optics, and the sample holder. In this section, the design steps involved in the fabrication of each of these components are described.
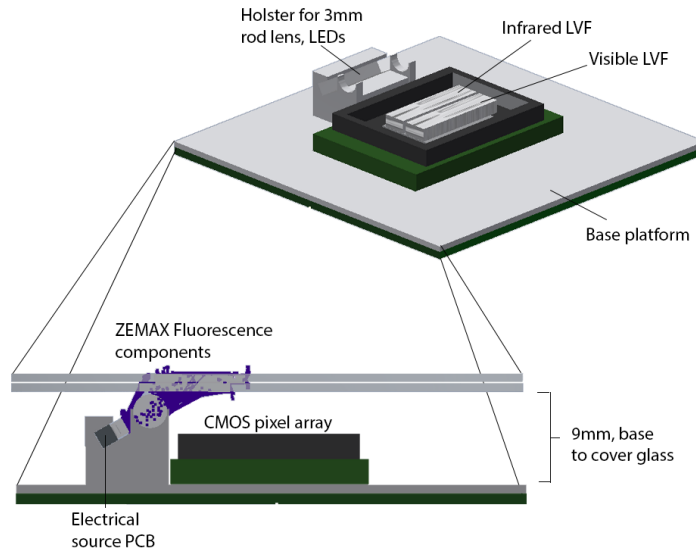

Figure 4.1: *(Top) Schematic of the aluminum base platform, used to fix the position of the light sources and rod lens around the CMOS sensor.*
(Bottom) Profile view of the platform, showing the light from the sources focused by the rod lens above the LVF detector.

4.2.1   Image Sensor and LVF

The NIR LVF is bonded to the sensor using a UV curable epoxy. The NIR LVF is also longer than the CMOS area, and as such must first be diced down

to size. As such, the NIR LVF is also characterized using a spectrophotometer (Varian Cary 5 G). The LVF can then be marked and diced in the same way as its visible counterpart, before being bonded onto the surface of the CMOS sensor using a UV-cured epoxy.

4.2.2   Illumination and Optics

Three red miniTOPLEDs (OSRAM) centered around a peak wavelength of 650 nm act as the systems illumination source to excite the fluorophores. These are similarly soldered onto a PCB. The LEDs need to be focused onto the sample in order to induce as intense an emission signal as possible. A rod lens sitting between the LEDs and the sample channel is used as a focusing element.

The spatial configuration of the illumination sources, the rod lens and the LVF is determined using Zemax OpticStudio. In order to successfully make a measurement, the LED light must be focused by the rod lens into the sample exciting the fluorophore. The resulting emission signal is then collected by the LVF-covered CMOS sensor. Zemax is used to determine the optimal position of each component in order to ensure that the system performs as desired.

The Zemax model is imported into standard CAD software (Inventor) in order to design a base platform to hold the components in place. The base must house the red LEDs, their PCB board, and the rod lens, while sitting around the CMOS image sensor. The fabricated apparatus is then screwed onto the CMOS-sensor chip, effectively surrounding the image sensor as illustrated in Figure 4.1. The PCB and rod lens are bonded to the support platform using UV-curable epoxy.

4.2.3   Sample Holder

The sample holders used are identical to those utilized in the absorption measurements in shape, basic design, and material used (Somos WaterClear Ultra 10122). However, since fluorescence experiments tend to use less sample material, channel sizes must be made smaller so as to not unnecessarily waste fluorophore. Additionally, the back of the fluidic channels is not coated in a

mirror, in order to limit the reflections of the incident light onto the CMOS sensor, which drowns out the weaker fluorescence signals. Smaller channel volumes result in more thoughtful channel placement, as the light needs to be focused in the center of the channel in order to achieve the best results. Using Zemax, the focal position of the incident light along the sample cartridge can be calculated. This data is used to design and fabricate cartridges with accurate channel positions.

4.2.4   Further Modifications

Early fluorescence experiments did not yield any positive data. The system was unable to resolve fluorescence signals that were measured using a portable spectrometer (Ocean Optics) as the fluorescence signal was still being drowned out by the incident signal. In order to address this issue, three design changes are made. The Zemax models are updated in order to account for inaccuracies in the final design. The data is used to fabricate a new sample cartridge with updated channel positions. Additionally, the aluminum cage is milled in order to reposition the LVF as close to the channel as possible. Finally, two 695 nm longpass filters (Thorlabs) are placed on top of the LVF in order to filter out any reflected red light. This allows for higher exposure times to be used without saturating the captured images. These modifications allow the system to be used to successfully resolve fluorescence signals.

4.3   Experiments

4.3.1   Calibration Experiment

Before fluorescence experiments can be planned, the NIR LVF-CMOS first has to be characterized to generate pixel-to-wavelength conversion. This is accomplished in a similar manner as described in Chapter 2.5. An incident white light source (Ocean Optics) is shined onto the LVF-CMOS system in a benchtop setup. Several filters are then placed in front of the light source producing different spectra, and images are captured using the LVF system.

Identical measurements are taken separately using the Ocean Optics spectrometer. The characteristic points of each spectrum are extracted for both sets of data. These features are used to generate a pixel-to-wavelength conversion shown in Figure 4.2.
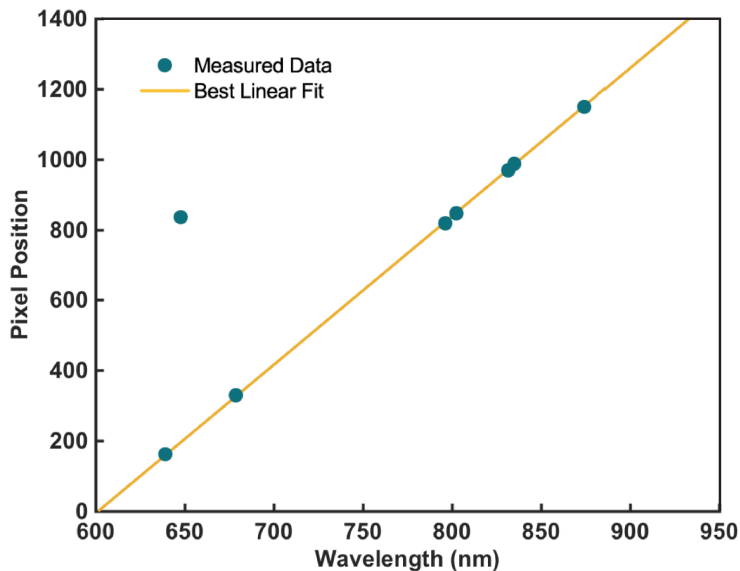

Figure 4.2: *Pixel position versus wavelength relationship for the NIR LVF-on-CMOS detector.*

4.3.2   Alexa Fluor 750 Dilution Sweep

Materials and Methods   A series of decreasing concentrations of an Alexa Fluor 750 solution is prepared. Alexa Fluor 750 is a NIR fluorophore that is excited around both the 650 nm and 750 nm wavelength regions, emitting a fluorescence signal around 780 nm as shown by its emission and excitation plots [28].

A 12.4 μg/mL solution is prepared by diluting the stock fluorophore with phosphate-buffered saline (PBS). Six sequential samples are prepared, each having the concentration of its predecessor. Three separate sets of seven concentrations are prepared in total. These are then individually tested using the modified fluorescence platform. Since fluorescence signals are much weaker than absorption ones, high exposure times are used to extract as much information as possible (up to 50 ms). In order to account for the noise

generated, a dark room image is taken before the samples are measured and is subtracted from the raw data during processing.
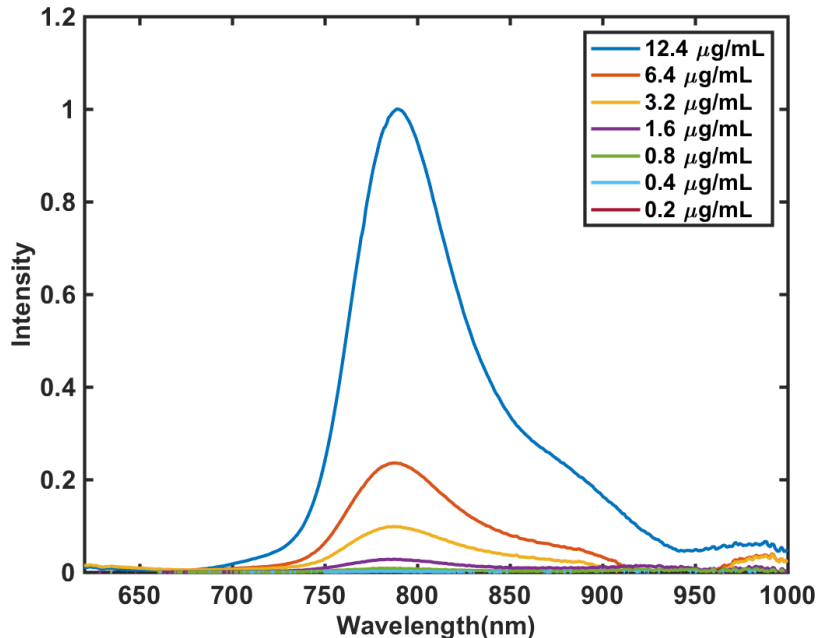

Figure 4.3: *Intensity spectra measured from successive concentrations of Alexa Fluor 750 diluted in PBS using the fluorescence platform.*

Results   Figure 4.3 shows the resulting intensity versus wavelength plots. A signal is resolved at concentrations as low as 0.8 μg/mL, showcasing the systems potential for fluorimetry. As expected, intensity increases with concentration. By running multiple sweeps, the gathered data can be used to determine a limit of detection for the system similar to the approach taken with the ELISA discussed in section 3.3.3.

While a dilution experiment is merely an initial attempt at characterizing the fluorescence platform, it certainly demonstrates the system's ability to resolve fluorescence signals.

CHAPTER 5

CONCLUSION

5.1   Summary of Results

Throughout this work, the design and fabrication of a set of smartphone-compatible compact biosensing systems are presented. Starting from a bench-top system, and culminating with compact absorption and fluorescence platforms, the evolution of the LVF-enabled biosensor is described, along with the experiments undertaken in order to properly characterize it.

First, an LVF-on-CMOS detector is conceived and tested in both absorption and fluorescence modalities, using benchtop characterization setups, utilizing free-space optics and external illumination sources. By way of a series of colorimetric and fluorimetry experiments, the LVF system is tested against both a portable spectrometer and an OSA, showing good agreement with both conventional spectroscopy tools. These experiments effectively illustrate the spectroscopic potential of an LVF-enabled detector, motivating the design and fabrication of miniaturized compact detection systems for both absorption and fluorescence spectroscopy.

The first of these, a compact absorption LVF-based platform, is fabricated and characterized by a series of liquid and solid phase experiments. A compact fluorescence platform is also designed and tested. The system is able to successfully resolve fluorescence signals, showing promising initial results.

While the LVF-enabled detection systems are unlikely to compete with laboratory spectrometers in terms of accuracy and measurement efficiency, their small footprint and ease of use make them a favorable candidate for point-of-care diagnostics. Their ability to spectroscopically discriminate between both solid and liquid phase samples and detect fluorescence could see them used in a wide variety of applications, ranging from simple curiosity to hard science.

5.2 Future Work

While the absorption system is thoroughly characterized, the fluorescence platform requires further testing. In addition to the Alexa Fluor 750 dilution sweeps, a Förster resonance energy transfer (FRET) molecular beacon (MB) assay experiment is planned, analogous to the ELISA performed with the absorption platform with the goal of contextualizing the system's ability via a routine biological test.

MB assays have been successfully run using smartphone spectroscopy systems [15] and represent a reasonable real-world application for a spectroscopic platform.

In order to provide a truly versatile point-of-care diagnostic platform, the fluorescence and absorption modalities are to be combined, resulting in an all-in-one system capable of performing a slew of different assays and tests. Such a system, illustrated in Figure 5.1, represents yet another step towards the development of a versatile smartphone-compatible biosensing platform.
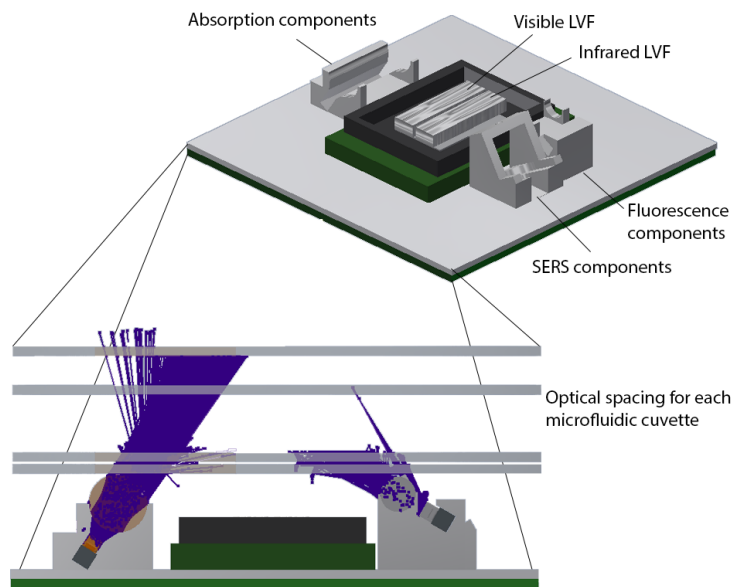

Figure 5.1: *Tentative design combining the absorption and fluorescence platforms into a single system (surface-enhanced Raman spectroscopy system no longer planned but also shown).*

REFERENCES

[1] R. Montes-Robles, M. E. Moragues, J.-L. Vivancos, J. Ibáñez, R. Fraile, R. Martínez-Máñez, and E. García-Breijo, "Colorimetric detection of hazardous gases using a remotely operated capturing and processing system," *ISA Transactions*, vol. 59, pp. 434–442, 2015.

[2] W. Zhao, M. M. Ali, S. D. Aguirre, M. A. Brook, and Y. Li, "Paper-based bioassays using gold nanoparticle colorimetric probes," *Analytical Chemistry*, vol. 80, no. 22, pp. 8431–8437, 2008.

[3] Y. Liu, Q. Teng, J. Hu, R. Sun, and H. Zhang, "Ferrocenyl-based unsymmetrical azines as multisignaling sensors for Hg2+, Cu2+ in aqueous environment," *Sensors and Actuators B: Chemical*, vol. 234, pp. 680–690, 2016.

[4] S. M. Z. Hossain and J. D. Brennan, "β-galactosidase-based colorimetric paper sensor for determination of heavy metals," *Analytical Chemistry*, vol. 83, no. 22, pp. 8772–8778, Nov 2011.

[5] X. Xue, F. Wang, and X. Liu, "One-step, room temperature, colorimetric detection of mercury (Hg 2+) using DNA/nanoparticle conjugates," *Journal of the American Chemical Society*, vol. 130, no. 11, pp. 3244–3245, 2008.

[6] Y. Song, W. Wei, and X. Qu, "Colorimetric biosensing using smart materials," *Advanced Materials*, vol. 23, no. 37, pp. 4215–4236, Oct 2011.

[7] O. R. Miranda, X. Li, L. Garcia-Gonzalez, Z.-J. Zhu, B. Yan, U. H. F. Bunz, and V. M. Rotello, "Colorimetric bacteria sensing using a supramolecular enzymenanoparticle biosensor," *Journal of the American Chemical Society*, vol. 133, no. 25, pp. 9650–9653, Jun 2011.

[8] K. D. Long, H. Yu, and B. T. Cunningham, "Smartphone instrument for portable enzyme- linked immunosorbent assays," *Biomedical Optics Express*, vol. 5, no. 11, p. 3792, Nov 2014.

[9] S. Ge, F. Liu, W. Liu, M. Yan, X. Song, and J. Yu, "Colorimetric assay of K-562 cells based on folic acid-conjugated porous bimetallic Pd@Au nanoparticles for point-of-care testing," *Chem. Commun.*, vol. 50, no. 4, pp. 475–477, 2014.

[10] S. K. Vashist, T. van Oordt, E. M. Schneider, R. Zengerle, F. von Stetten, and J. H. Luong, "A smartphone-based colorimetric reader for bioanalytical applications using the screen-based bottom illumination provided by gadgets," *Biosensors and Bioelectronics*, vol. 67, pp. 248–255, 2015.

[11] N. Sattarahmady, A. Movahedpour, H. Heli, and G. Hatam, "Gold nanoparticles-based biosensing of Leishmania major kDNA genome: Visual and spectrophotometric detections," *Sensors and Actuators B: Chemical*, vol. 235, pp. 723–731, 2016.

[12] V. Gubala, L. F. Harris, A. J. Ricco, M. X. Tan, and D. E. Williams, "Point of care diagnostics: status and future," *Analytical Chemistry*, vol. 84, no. 2, pp. 487–515, 2012.

[13] Ocean Optics, Spark-VIS, Datasheet.

[14] Hamamatsu Photonics, Micro-spectrometer C12666MA, Datasheet.

[15] H. Yu, Y. Tan, and B. T. Cunningham, "Smartphone fluorescence spectroscopy," *Analytical Chemistry*, vol. 86, no. 17, pp. 8805–8813, Sep 2014.

[16] D. Gallegos, K. D. Long, H. Yu, P. P. Clark, Y. Lin, S. George, P. Nath, and B. T. Cunningham, "Label-free biodetection using a smartphone," *Lab on a Chip*, vol. 13, no. 11, p. 2124, 2013.

[17] A. Emadi, H. Wu, G. De Graaf, K. Hedsten, P. Enoksson, J. H. Correia, and R. F. Wolffenbuttel, "An UV linear variable optical filter-based micro-spectrometer," *Procedia Engineering*, vol. 5, pp. 416–419, 2010.

[18] A. Emadi, H. Wu, G. De Graaf, and R. Wolffenbuttel, "Design and implementation of a sub-nm resolution microspectrometer based on a Linear-Variable Optical Filter," *Optics Express*, vol. 20, no. 1, p. 489, Jan 2012.

[19] A. Emadi, H. Wu, G. De Graaf, and R. F. Wolffenbuttel, "IR microspectrometers based on linear-variable optical filters," *Procedia Engineering*, vol. 25, pp. 1401–1404, 2011.

[20] M. Ghaderi, N. P. Ayerden, A. Emadi, P. Enoksson, J. H. Correia, G. De Graaf, and R. F. Wolffenbuttel, "Design, fabrication and characterization of infrared lvofs for measuring gas composition," *Journal of Micromechanics and Microengineering*, vol. 24, no. 8, 2014.

[21] J. T. Verdeyen, *Laser Electronics*. Prentice Hall, 1995.

[22] W. T. Silfvast, *Laser Fundamentals*. Cambridge, 2004.

[23] S. L. Chuang, *Physics of Photonic Devices*. Wiley, 2009.

[24] A. Emadi, H. Wu, S. Grabarnik, G. De Graaf, and R. F. Wolffenbuttel, "IC-compatible fabrication of linear variable optical filters for microspectrometer," *Procedia Chemistry*, vol. 1, no. 1, pp. 1143–1146, 2009.

[25] R. Seddon, B. Swaby, R. Ryall, S. Solberg, and E. Anthon, "Monolithic linear variable filter and method of manufacture," Feb 1999, US Patent 5,872,655.

[26] R. H. Garrett and C. M. Grisham, *Biochemistry*. Cengage, 1995.

[27] J. Mertz, *Introduction to Optical Microscopy*. Roberts and Company Publishers, 2010.

[28] Invitrogen, *The Molecular Probes Handbook*, 2010.

[29] Y. Wan, J. A. Carlson, B. A. Kesler, W. Peng, P. Su, S. A. Al-Mulla, S. J. Lim, A. M. Smith, J. M. Dallesasse, and B. T. Cunningham, "Compact characterization of liquid absorption and emission spectra using linear variable filters integrated with a CMOS imaging camera," *Scientific Reports*, vol. 6, p. 29117, 2016.

[30] D. L. Harp, Hach Co., Technical Information Series, vol. 17, 2002.

[31] A. M. Smith and S. Nie, "Compact quantum dots for single-molecule imaging," *Journal of Visualized Experiments*, no. 68, Oct 2012.

[32] S. J. Lim, M. U. Zahid, P. Le, L. Ma, D. Entenberg, A. S. Harney, J. Condeelis, and A. M. Smith, "Brightness-equalized quantum dots," *Nature Communications*, vol. 6, p. 8210, Oct 2015.

[33] Y. Wan, J. A. Carlson, S. A. Al-Mulla, W. Peng, K. D. Long, B. A. Kesler, P. Su, J. M. Dallesasse, and B. T. Cunningham, submitted to *Sensors and Actuators B: Chemical*.

[34] J. Gibbs, Corning Life Sciences, *Selecting the Detection SystemColorimetric, Fluorescent, Luminescent Methods*, ELISA Technical Bulletin, vol. 5.

[35] CUSABIO, *Human Fetal Fibronectin (fFN) ELISA Kit*, Instruction Manual.